Available online at www.sciencedirect.com

SCIENCE DIRECT

Genomics 84 (2004) 555–564

GENOMICS

www.elsevier.com/locate/ygeno

# Targeted point mutagenesis of mouse *Kcnq1:* phenotypic analysis of mice with point mutations that cause Romano-Ward syndrome in humans

Mathew C. Casimiro[a,1], Bjoern C. Knollmann[b,1], Ebenezer N. Yamoah[c], Liping Nie[c], Jay C. Vary Jr.[a,d], Syevda G. Sirenko[b], Anne E. Greene[b], Alexander Grinberg[a], Sing Ping Huang[a], Steven N. Ebert[b], Karl Pfeifer[a,*]

[a]*Laboratory of Mammalian Genes and Development, NICHD/National Institutes of Health, Building 6B Room 2B-206, 9000 Rockville Pike, Bethesda, MD 20892, USA*

[b]*Department of Pharmacology, Georgetown University Medical Center, Washington, DC 20007, USA*

[c]*Center for Neuroscience, Department of Otolaryngology, University of California at Davis, 1544 Newton Court, Davis, CA 95616, USA*

[d]*Howard Hughes Medical Institute–NIH Research Scholar Program, Bethesda, MD 20872, USA*

Received 23 February 2004; accepted 9 June 2004

**Abstract**

Inherited long QT syndrome is most frequently associated with mutations in *KCNQ1*, which encodes the primary subunit of a potassium channel. Patients with mutations in *KCNQ1* may show only the cardiac defect (Romano-Ward syndrome or RWS) or may also have severe deafness (Jervell and Lange-Nielsen syndrome or JLNS). Targeted disruption of mouse *Kcnq1* models JLNS in that mice are deaf and show abnormal ECGs. However, the phenotype is broader than that seen in patients. Most dramatically, the inner ear defects result in a severe hyperactivity/circling behavior, which may influence cardiac function. To understand the etiology of the cardiac phenotype in these mice and to generate a potentially more useful model system, we generated new mouse lines by introducing point mutations associated with RWS. The *A340E* line phenocopies RWS: the repolarization phenotype is inherited in a dominant manner and is observed independent of any inner ear defect. The *T311I* line phenocopies JLNS, with deafness associated with inner hair cell malfunction.


*Keywords:* Romano-Ward syndrome; RWS; JLNS; Long QT; Kcnq1; Mice; Genetics; Deafness

Long QT syndrome (LQTS) is an abnormality in cardiac ventricular repolarization characterized by QT interval prolongation and abnormal T-waves on an electrocardiogram (ECG). LQTS patients are susceptible to polymorphic ventricular tachycardia and torsades de pointe. These can cause syncopal episodes and sudden death in young, otherwise healthy individuals. The past several years have heralded dramatic progress in understanding the molecular biology of LQTS and have led to the notion that LQT is a channelopathy caused by mutations in genes coding for ion channels important in cardiac function [1,2].

To date six genes have been identified in inherited LQT patients[3–8]. The most common cause of inherited LQTS is mutation of the *KCNQ1* gene (LQT1), which encodes the primary channel-forming α-subunit of a voltage-gated potassium channel [9]. KCNQ1 can associate with β-subunits of the KCNE family. To date, the KCNE family consists of five members (KCNE1–KCNE5) [6,10–14], each of which is capable of associating with KCNQ1 and forming $K^+$ channels with distinct electrophysiological properties predicted to be involved in diverse roles in different tissues. For instance, when KCNQ1 pairs with KCNE1, the channel is transformed into producing the slowly activating time-dependant potassium current, $I_{Ks}$, found in cardiac myocytes and specialized epithelial cells of the inner ear [15–17].

* Corresponding author.
*E-mail address:* pfeiferk@mail.nih.gov (K. Pfeifer).
[1] These authors contributed equally to this work.

0888-7543/$ - see front matter © 2004 Elsevier Inc. All rights reserved.
doi:10.1016/j.ygeno.2004.06.007

Mutations in *KCNQ1* (*LQT1*) and *KCNE1* (*LQT5*) are associated with two clinical forms of LQTS, Romano-Ward syndrome (RWS) and Jervell Lange-Nielsen syndrome (JLNS). JLNS is characterized by profound sensorineural deafness in association with a more severe cardiac phenotype that causes a higher incidence of sudden death [18]. Genotype/phenotype correlations in LQTS patients reveal a complex inheritance pattern: the deafness is inherited in a recessive fashion; however, the LQT phenotype in the two syndromes is usually inherited as a dominant trait with varying degrees of penetrance [19].

Insight into why JLNS patients are deaf came from postmortem studies, which revealed inner ear morphology changes that are consistent with the lack of endolymph in the membranous labyrinth of the inner ear [20]. Endolymph is a $K^+$-rich fluid that bathes the hair cells in the vestibular and auditory compartments and is essential for inner ear function. The stria vascularis of the cochlea and dark cells in the vestibular apparatus are known to be responsible for the production of endolymph fluid. Both Kcnq1 and Kcne1 have been localized to these regions and $I_{Ks}$ is a candidate for endolymph secretion [17,21–24]. A requirement for $I_{Ks}$ is further supported by the deafness and vestibular defects found in *Kcnq1*$^{-/-}$ and *Kcne1*$^{-/-}$ mice[25–27].

We previously published work on the targeted disruption of the mouse *Kcnq1* gene that produced a model for JLNS. In vivo ECG analysis revealed that, like JLNS patients, the *Kcnq1*$^{-/-}$ mice display long QT intervals and altered T-wave morphology [25]. The mice are deaf, and histological analyses revealed gross morphological anomalies of the inner ear due to a drastic reduction in the volume of endolymph [25,26]. However, the mice also displayed defects not found in human JLNS patients. The ECG phenotype included P-wave changes and an increase in QRS amplitude. Furthermore, the inner ear dysfunction causes a hyperactive behavioral defect (shaker/waltzer) characterized by almost continual circling and rapid head bobbing. This behavioral phenotype is specific to mice and is not displayed by JLNS patients with equally profound defects in inner ear function. Presumably, humans have more robust compensatory mechanisms. Finally, the stomachs of *Kcnq1*$^{-/-}$ mice were grossly enlarged due to gastric hyperplasia [26].

We were particularly struck with the shaker/waltzer phenotype since it seemed plausible that some of the cardiac phenotypes might be secondary to the pronounced hyperactivity of these mice. In this study, we attempt to separate the ECG phenotype from the inner ear by taking advantage of the extensive human genetic studies. Specifically, we have engineered point mutations into mouse *Kcnq1* that we hypothesized would generate a RWS mouse and thereby allow us to examine the cardiac defect without the added complexity of the inner ear phenotype. We report here on the construction and analysis of three novel lines with point mutations in *Kcnq1* that cause RWS in humans. Mice carrying the *A340E* mutation have normal hearing but a long QT and therefore model patients with RWS. This mouse demonstrates that the long QT phenotype in our models is independent of an inner ear defect. Mice homozygous for *T311I* display shaker/waltzer, deafness, and balance problems. Histological examination revealed that the auditory and vestibular defects are caused by collapse of the membranous labyrinth and degeneration of the sensory epithelium. The *Kcnq1*$^{T311I/T311I}$ mice exhibit a long QT, increased QRS amplitude, and mild T-wave area changes and therefore resemble patients with JLNS. Together these mice suggest that the QRS amplitude changes are likely a consequence of the hyperactivity associated with inner ear dysfunction.

## Results

### *Generation of T311I, A340V, and A340E Kcnq1 mice*

Mouse and human KCNQ1 proteins are highly similar across their entire length [28]. We chose to mutagenize amino acids *T311* and *A340* (previously called *T247* and *A276*) of mouse Kcnq1. These residues are present in the pore domain and S6 transmembrane domain, respectively [7,15] (Fig. 1). Our changes mimic missense mutations found in human RWS patients, *T312I*, *A341V*, and *A341E* [7,29–32].

We generated these mice via a two-step process so that the *neomycin* cassette used for positive selection in cell culture was removed prior to analysis of the mice (Fig. 2). Mice heterozygous for each mutation were bred to obtain *Kcnq1*$^{+/+}$, *Kcnq1*$^{pt/+}$, and *Kcnq1*$^{pt/pt}$ progeny (Fig. 2D). Homozygous and heterozygous *T311I, A340V*, and *A340E* mice were each present at normal Mendelian frequencies at weaning and at 4 months of age. Similar

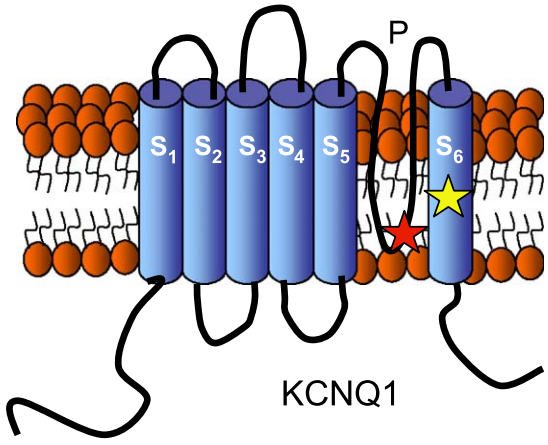


Fig. 1. Cartoon of predicted Kcnq1 structure with the locations of amino acids T311 (red star) and A340 (yellow star), mutated in this study. Kcnq1 consists of six transmembrane domains ($S_1$–$S_6$) and a pore domain (P) [7].

levels of mRNA were detected in wild-type, heterozygous, and homozygous *T311I*, *A340V*, and *A340E* mice, indicating that the mRNA expression from the three mutated alleles is comparable to that from the wild-type allele. A representative Northern blot is depicted in Fig. 2E. Finally, sequencing of amplified cDNAs from these mice confirmed the presence of the mutation in correctly spliced mRNA (data not shown).

*Behavioral analysis*

When the mice were examined at postnatal day 30, *Kcnq1*$^{+/T311I}$ mice and the heterozygous and homozygous *A340E* and *A340V* mice appeared normal and exhibited startle in response to a hand clap (Preyer's reflex). However, the *Kcnq1*$^{T311I/T311I}$ mice exhibited hyperactivity characterized by rapid head bobbing and intermittent bidirectional circling. This behavior, which mimics that of the *Kcnq1*$^{-/-}$ mice, is symptomatic of inner ear defects and usually referred to as shaker/waltzer phenotype. *Kcnq1*$^{T311I/T311I}$ mice did not show Preyer's reflex, indicating that their hearing was impaired.

*Auditory and vestibular analysis*

A series of auditory and vestibular analyses was performed to evaluate more precisely the inner ear function in these mice. Specifically, we evaluated mice carrying the *T311I* allele, which caused shaker/waltzer syndrome when homozygous, and the *A340E* mutation, which appeared at first glance to have no inner ear phenotype. We did not do a complete characterization of the other phenotypically silent mutation, *A340V*, because preliminary cardiac studies suggested that even mice homozygous for this mutation lacked a significant cardiac-related phenotype (see below) and therefore these mice were not good phenocopies of human RWS.

We first evaluated audition by performing auditory brainstem recordings (ABR). Consistent with their normal Preyer's reflex, the ABR of *A340E* mice is indistinguishable from that of their wild-type littermates (Figs. 3A and 3B). In contrast there were no characteristic ABR waveforms detected from *Kcnq1*$^{T311I/T311I}$ mice even at 100-dB clicks and 8-, 16-, and 32-kHz pure tones (representative trace in Fig. 3C). Fig. 3D summarizes ABR thresholds in *T311I*

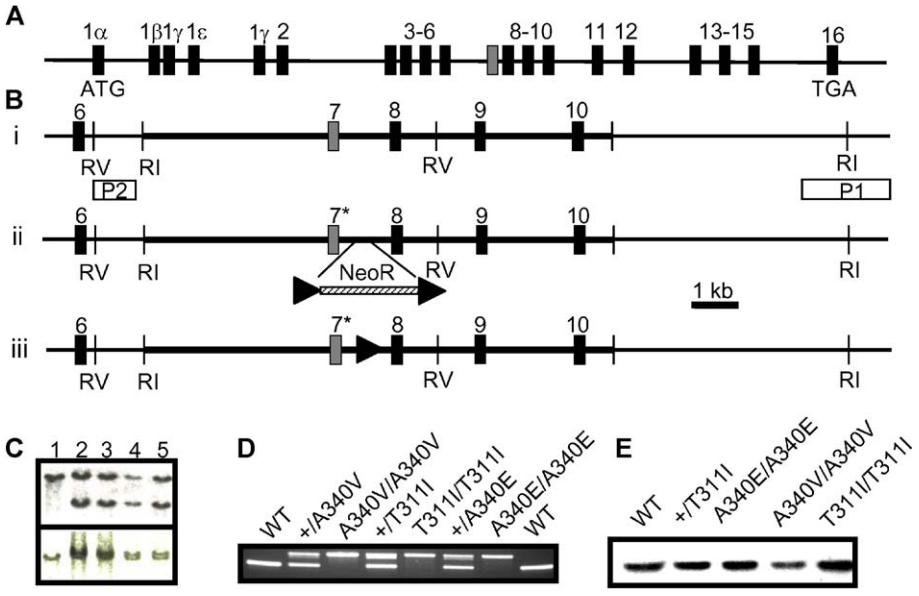


Fig. 2. Construction of the *T311I, A340E*, and *A340V* alleles of *Kcnq1*. (A) Cartoon of the 300-kb mouse *Kcnq1* gene. Exons are depicted as filled black boxes, except for exon 7, which is indicated in gray. The translational start and stop for the major *Kcnq1* isoform are indicated. (B) The three *Kcnq1* alleles were each constructed in a two-step process by mutagenesis of the wild-type chromosome (i). First, *T311I-NEO, A340E-NEO*, and *A340V-NEO* (ii) were each generated by targeted mutagenesis in RI embryonic stem cells. These chromosomes each carry single base pair changes in exon 7 (exon 7*) as well as a 1.1-kb insertion conferring resistance to G418 (*NeoR*) that is flanked with *loxP* sites (closed arrowheads). Correctly targeted cell lines were used to generate mutant mice. Second, *T311I, A340E*, and *A340V* alleles (iii) were generated in vivo via Cre recombination. Thus the mice characterized in this study carry only single base pair changes in exon 7 and a small insertion of a single *loxP* element in the intron separating exons 7 and 8. RI, *Eco*RI; RV, *Eco*RV. (C) Identification of mutant cell lines by Southern analyses. Clones correctly targeted on the 3′ end carry a 10-kb *Eco*RI fragment in addition to the 16-kb band characteristic of the wild-type chromosome (top). Clones correctly targeted on the 5′ end carry a 10.6-kb *Eco*RV fragment in addition to the 9.5-kb band characteristic of the wild-type chromosome (bottom). DNAs were prepared from wild-type RI cells (lane 1) and from mutant cell lines carrying the *A311I-NEO* allele (lanes 2 and 3), the *A340E-NEO* allele (lane 4), or the *A340V-NEO* allele (lane 5). The 5′ ("P1") and 3′ ("P2") probes are indicated as open rectangles in B. (D) Identification of mutant mice by PCR analysis. Founder mice were crossed with transgenic females in which the Cre *recombinase* gene was expressed under the control of the *EIIa* promoter. Upon amplification with primers spanning the *NeoR* insertion site, wild-type and mutant chromosomes yield products of 388 and 508 bp, respectively. (E) Mutant chromosomes express *Kcnq1* RNA at wild-type levels. RNA was prepared from 12- to 14-week mouse hearts and quantitated by Northern blot analysis. RNA loading was normalized by staining for ribosomal RNAs. A representative Northern is depicted. However, for each mutation RNA levels from at least two mutant animals were compared with RNAs from wild-type and heterozygous littermates.

mice and demonstrates that every *Kcnq1*$^{T311I/T311I}$ mouse was deaf at all frequencies tested.

Since ABR data alone are not sufficient evidence to categorize the defect as specific to hair cell malfunction, we initiated a series of distortion product otoacoustic emission (DPOAE) studies. DPOAEs are acoustic measurements of outer hair cell activity. Fig. 3E shows DPgrams from homozygous *A340E* and *T311I* mice and demonstrates that *Kcnq1*$^{A340E/A340E}$ and wild-type mice exhibited similar DPs. The DPgrams from *Kcnq1*$^{T311I/T311I}$ mice were similar to recordings from the noise floor. Combining the data from both ABR and DPOAE techniques indicates the auditory defect in *Kcnq1*$^{T311I/T311I}$ mice is caused by cochlea defects.

To assess vestibular function in the point-mutant mice a swim test was conducted. Heterozygous and homozygous *A340E* mice behaved like wild-type mice (Fig. 3F). However, all the *Kcnq1*$^{T311I/T311I}$ mutant mice showed abnormal swimming behavior associated with lack of orientation: when placed in water, the mutants spiraled underwater in a corkscrew fashion and had to be rescued immediately from drowning. As an alternative assay, mice were placed on a cylinder connected to a variable-speed motor that runs from 0 to 15 rpm and each animal's ability to balance on both the stationary and the rotating cylinder was scored (Fig. 3F). *Kcnq1*$^{A340E/A340E}$ mice behaved like wild-type mice; however, *Kcnq1*$^{T311I/T311I}$ mice performed so poorly that often they failed to balance on the cylinder while stationary.

Finally, morphological examination of the inner ear was done to determine whether anatomical differences would account for impaired hearing and vestibular function. Midmodular sections of the cochlea from adult animals revealed that in *Kcnq1*$^{T311I/T311I}$ mice Reissner's membrane had completely collapsed, lying against the lateral wall and on top of the spiral limbus and tectoral membrane of the organ of Corti (Fig. 4A). In addition we observed degeneration of the inner and outer hair cells. The morphology of the cochlea from *Kcnq1*$^{A340E/A340E}$ mice and wild-type mice appeared normal (Figs. 4B and 4C). The vestibular apparatus is composed of the semicircular canals, which detect angular acceleration, and two sac-like swellings, utricle and saccule, which are sensitive to linear acceleration. Sections of the utricle from *Kcnq1*$^{T311I/T311I}$

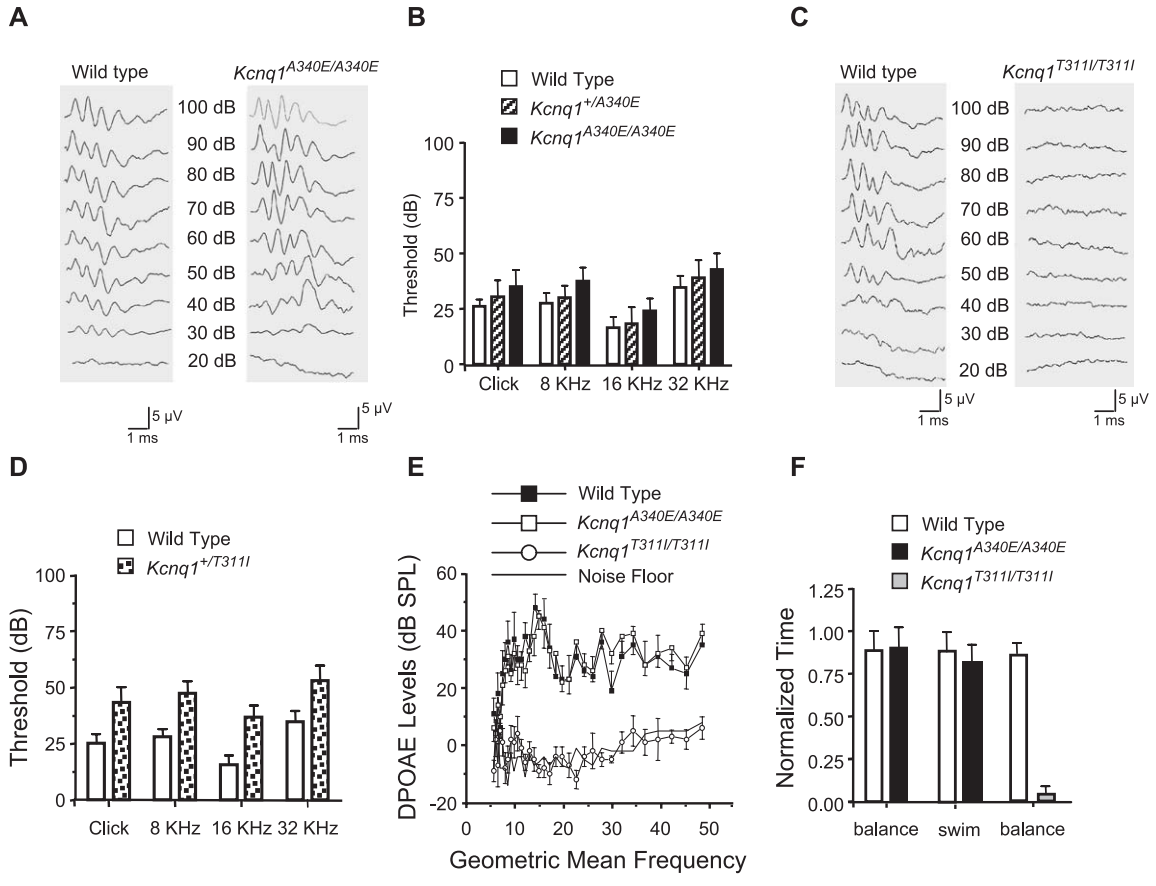


Fig. 3. (A) Representative ABR waveforms from *Kcnq1*$^{A340E/A340E}$ mice compared to wild-type littermates. (B) Average ABR threshold for heterozygous ($n = 19$) and homozygous ($n = 19$) *A340E* mice versus age-matched wild-type mice ($n = 19$). (C) Representative ABR waveforms from *Kcnq1*$^{T311I/T311I}$ mice compared to wild-type littermate. (D) Average ABR thresholds for Kcnq1$^{+/T311I}$ ($n = 16$) mice compared to wild-type littermates ($n = 16$). *Kcnq1*$^{T311I/T311I}$ mice showed no response. (E) DPgrams for wild-type and homozygous *T311I* and *A340E* mice. The DPOAE levels for *Kcnq1*$^{T311I/T311I}$ mice are indistinguishable from background (noise floor). (F) To test gross vestibular function of point-mutant mice, a balance test was performed. Mice were generated as described under Methods and assayed at 8 to 10 weeks of age.

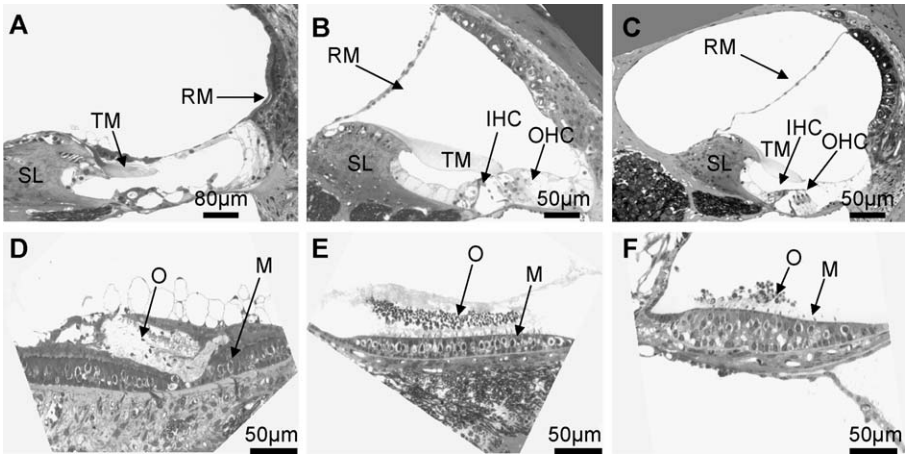


Fig. 4. Details of the cochlea and utricle from adult wild-type and homozygous *T311I* and *A340E* mice. (A) In *Kcnq1*$^{T311I/T311I}$ mice, Reissner's membrane (RM) has collapsed and is lying on the spiral limbus (SL) and tectoral membrane (TM) and along the lateral wall of the cochlea. Note the degeneration of the inner hair cells (IHC) and outer hair cells (OHC). (B, C) In wild-type and homozygous *A340E* mice the gross morphology of the cochlea appears normal. (D) The epithelium has collapsed onto the sensory cells of the utricle in the *Kcnq1*$^{T311I/T311I}$ mice. (E, F) However, the utricle in the wild-type and *Kcnq1*$^{A340E/A340E}$ mice appears normal. The otoconia (O) are embedded in the otolithic membrane (OM) overlying the neuroepithelium of the macula (M); tufts of hair bundles and corresponding cell bodies are identifiable. Mice were generated as described under Methods and sacrificed at 10 weeks. Representative samples that include comparisons of wild-type and mutant littermates are depicted. However, the histology of wild-type littermates for *T311I* and *A340E* could not be distinguished and therefore only one wild-type control is shown.

mice revealed that the membranous labyrinth had collapsed onto the sensory epithelium (Fig. 4D), while the *Kcnq1*$^{A340E/A340E}$ mice look normal (Figs. 4E and 4F). In addition we observed hair cell degeneration in the sensory epithelium of the saccule, utricle, and semicircular canals. This evidence corroborates previous histological data from *Kcnq1*$^{-/-}$ and *Kcne1*$^{-/-}$ mice and further supports the notion that $I_{Ks}$ is essential to inner ear homeostasis.

In sum, our analyses show that mice homozygous for *T311I* show severe inner ear defects in structure and function, while mice that are either heterozygous or homozygous for the *A340E* mutation cannot be distinguished from wild-type littermates.

### *Analysis of cardiac function in point mutants*

Since the primary goal of this study was to determine the relationship between the cardiac and the hyperactive defects, we were especially interested in comparing cardiac function in *A340E* and *T311I* mice. Examples of ECGs recorded from *Kcnq1*$^{+/A340E}$ and *Kcnq1*$^{A340/A340E}$ mice compared to wild-type mice are shown in Fig. 5. Summaries of the results from multiple mice are presented in Table 1. *Kcnq1*$^{+/A340E}$ mice display long JT, QT, and QTc intervals that are a hallmark of LQTS patients (Fig. 5) (Table 1). These results show that the *A340E* mutation exerts a dominant negative affect on channel function. Homozygosity of the mutation had a more profound effect on channel dysfunction, leading to a longer QT and dramatically increasing the statistical significance of the changes in these mice. The cardiac phenotype in both homozygous and heterozygous mice is restricted to a defect in repolarization, as we observed no changes in P- or QRS-waves. The phenotype of the *A340E* mice demonstrates directly that the long QT in the mouse models is independent of the hyperactive behavior of the shaker/waltzer mouse.

In a preliminary analysis of *A340V* mice, neither heterozygous nor homozygous mice demonstrated any significant increase in QRS amplitude, T-wave area, or QT interval (data not shown). We surmise the heart is largely unaffected by the *A340V* mutation.

Finally, we examined the cardiac phenotype of *T311I* mice, the line that shows deafness and hyperactivity in the homozygous state. *Kcnq1*$^{+/T311I}$ mice are asymptomatic and look like wild-type littermate controls (Table 1). Hence the *T311I* mutation does not exert an observable dominant negative affect on the heart. However, analysis of the *Kcnq1*$^{T311I/T311I}$ mice revealed a prevalent cardiac phenotype. First, these mice show prolongation of the JT, QT, and QTc intervals, indicating defects in ventricular repolarization (Fig. 5) (Table 1). Second, just like the *Kcnq1*$^{-/-}$ mice, but unlike the *A340E* mice, these animals show a dramatic increase in QRS amplitude and T-wave area. These data show that the *T311I* mutation can phenocopy JLNS since the mice are deaf and show long QT intervals. These data also suggest that the increased QRS amplitude is associated with the hyperactivity shaker/waltzer phenotype. No arrhythmias were observed in any of the recorded mice.

### *Physical and anatomical analysis of the point mutants*

After acquisition of the ECG data, we recorded body weight, ventricular weight, and atrial weight of each mouse, as these are each known to affect ECG parameters. The *Kcnq1*$^{T311I/T311I}$ mice are 27% lighter on average than their

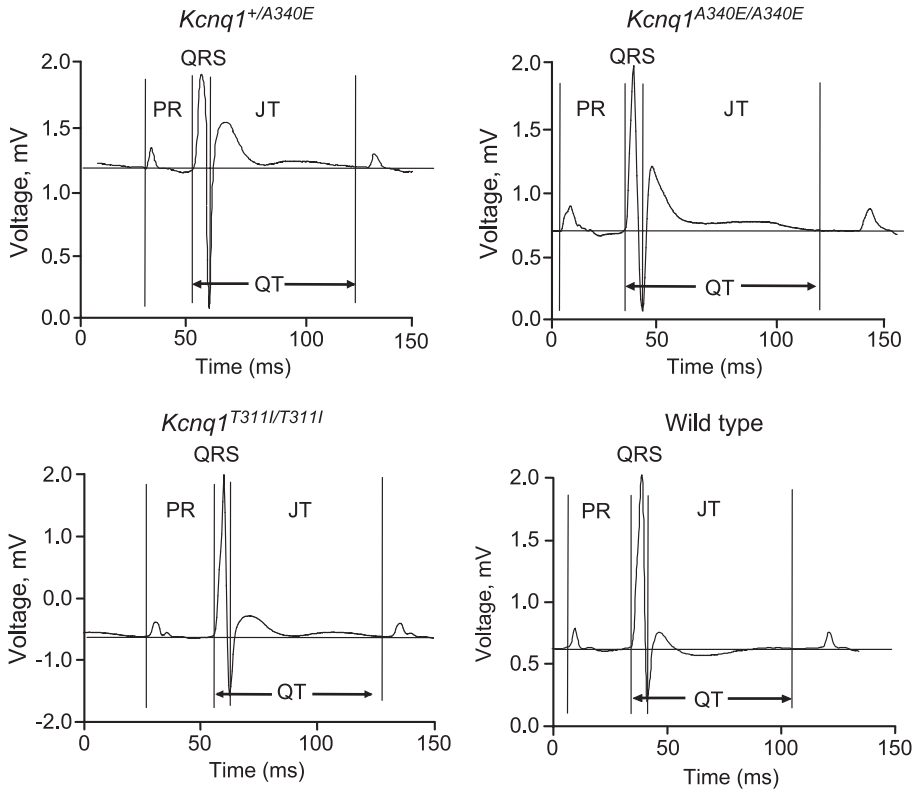


Fig. 5. Representative surface ECG traces (lead II) recorded in vivo from a heterozygous (upper left trace) and a homozygous *A340E* mouse (upper right trace), a homozygous *T311I* mouse (lower left trace), and a wild-type mouse (lower right trace). The traces indicate several ECG parameters measured during analysis. Note the long QT interval for the point-mutant mice compared to the wild-type mouse and the magnitude of the QRS amplitude in the homozygous *T311I* mouse. The depicted tracings were selected as representative of the particular phenotype although variation from mouse to mouse was noted within each genotype as indicated in Table 1. Mice were generated as described under Methods and in the footnote to Table 1.

wild-type littermates (Table 2). A gender bias in the pools did not account for the difference since it was present in both male (30 ± 3 and 27 ± 2 g for WT and *Kcnq1*$^{T311I/T311I}$ mice, respectively; $p < 0.05$) and female mutant mice (22 ± 3 and 19 ± 2 g for WT and *Kcnq1*$^{T311I/T311I}$ mice, respectively; $p < 0.01$). Both *T311I* and *A340E* mice

Table 1
ECG parameters for wild-type and mutant mice

| Parameter | *WT* ($n$ = 28) | *+/A340E* ($n$ = 21) | *A340E/A340E* ($n$ = 21) | $p$ value vs Het | $p$ value vs Homo | WT ($n$ = 28) | *+/T311I* ($n$ = 19) | *T311I/T311I* ($n$ = 21) | $p$ value vs Het | $p$ value vs Homo |
|---|---|---|---|---|---|---|---|---|---|---|
| RR (ms) | 103 ± 2 | 105 ± 2 | 108 ± 3 | 0.45 | 0.12 | 103 ± 2 | 108 ± 2 | 105 ± 2 | 0.7 | 0.60 |
| $P_{amp}$ (mV × $10^{-2}$) | 20 ± 1 | 21 ± 1 | 19 ± 1 | 0.22 | 0.56 | 23 ± 1 | 23 ± 1 | 24 ± 1 | 0.96 | 0.33 |
| P-wave duration (ms) | 11 ± 0.2 | 10 ± 0.2 | 11 ± 0.3 | 0.26 | 0.81 | 11 ± 0.3 | 11 ± 0.3 | 11 ± 0.3 | 0.77 | 0.77 |
| P-wave area (V ms × $10^{-1}$) | 10 ± 1 | 11 ± 1 | 10 ± 1 | 0.95 | 0.81 | 12 ± 1 | 12 ± 1 | 13 ± 1 | 0.80 | 0.32 |
| PR (ms) | 32 ± 1 | 30 ± 1 | 29 ± 1 | 0.05 | 0.07 | 31 ± 1 | 32 ± 1 | 30 ± 1 | 0.70 | 0.10 |
| QRS duration (ms) | 8.8 ± 0.2 | 8.6 ± 0.2 | 8.6 ± 0.1 | 0.56 | 0.62 | 8.5 ± 0.2 | 8.7 ± 0.3 | 8.1 ± 0.2 | 0.40 | 0.07 |
| QRS amplitude (vV × $10^{-2}$) | 198 ± 11 | 205 ± 7 | 213 ± 12 | 0.59 | 0.33 | 195 ± 10 | 210 ± 11 | 259 ± 13 | 0.32 | **<0.001** |
| JT (ms) | 63 ± 1 | 67 ± 1 | 70 ± 2 | **0.02** | **<0.001** | 63 ± 1 | 65 ± 1 | 68 ± 1 | 0.37 | **0.02** |
| QT (ms) | 72 ± 1 | 76 ± 1 | 79 ± 2 | **0.03** | **0.001** | 71 ± 1 | 73 ± 1 | 76 ± 2 | 0.31 | **0.04** |
| QTc (ms) | 71 ± 1 | 74 ± 1 | 76 ± 1 | **0.03** | **0.003** | 70 ± 1 | 71 ± 1 | 74 ± 1 | 0.81 | **0.03** |
| T-wave area (mV × $10^{-1}$) | 65 ± 4 | 77 ± 7 | 75 ± 9 | 0.12 | 0.23 | 69 ± 5 | 64 ± 6 | 94 ± 6 | 0.48 | **0.002** |

All data are presented as means ± standard error of the mean. Data sets from mutant mice were compared to those of wild-type mice using Student's $t$ test. $p$ values <0.05 are in bold. Het, heterozygous; Homo, homozygous; WT, wild type.

Table 2
Decreased body weight correlates with hyperactivity but not with gastric hyperplasia

| Parameter | *WT* ($n$ = 28) | *+/A340E* ($n$ = 21) | *A340E/A340E* ($n$ = 21) | $p$ value Het | $p$ value Homo | WT ($n$ = 28) | *+/T311I* ($n$ = 19) | *T311I/T311I* ($n$ = 21) | $p$ value Het | $p$ value Homo |
|---|---|---|---|---|---|---|---|---|---|---|
| Body (g) | 29.5 ± 1 | 29.5 ± 1 | 29.6 ± 1.2 | 0.95 | 0.94 | 27.9 ± 0.9 | 24.6 ± 1 | 21.9 ± 0.9 | 0.11 | **<0.001** |
| Ventricles (mg) | 133 ± 5 | 131 ± 6 | 134 ± 7 | 0.79 | 0.88 | 109 ± 4 | 104 ± 4 | 100 ± 4 | 0.34 | 0.12 |
| Heart/body ratio | 4.5 ± 0.4 | 4.4 ± 0.1 | 4.5 ± 0.1 | 0.92 | 0.92 | 4.1 ± 0.1 | 4.2 ± 0.1 | 4.6 ± 0.1 | 0.20 | **<0.001** |
| Atria (mg) | 7.7 ± 0.4 | 7.1 ± 0.5 | 8.2 ± 0.6 | 0.35 | 0.51 | 5.9 ± 0.4 | 4.8 ± 0.3 | 5.5 ± 0.4 | **0.03** | 0.46 |
| Atria/body ratio | 0.26 ± 0.01 | 0.24 ± 0.01 | 0.26 ± 0.02 | 0.19 | 0.98 | 0.22 ± 0.01 | 0.20 ± 0.01 | 0.25 ± 0.01 | 0.07 | **0.04** |
| Stomach (mg) | 164 ± 7 | 168 ± 6 | 392 ± 34 | 0.62 | **<0.001** | 123 ± 4 | 144 ± 6 | 320 ± 17 | **0.005** | **<0.001** |

All data are presented as means ± standard error of the mean. Data sets were compared using Student's $t$ test. $p$ values <0.05 are in bold. Het, heterozygous; Homo, homozygous; WT, wild type.

displayed the gastric hyperplasia noted in *Kcnq1*$^{-/-}$ mice. Thus the difference in body weight in *T311I* is best explained by hyperactivity, which could be viewed as an extreme form of exercise.

## Discussion

We previously published a model for long QT in which disruption of *Kcnq1* leads to a mouse that resembles patients with JLNS. The *Kcnq1*$^{-/-}$ mice are deaf [26] and ECG analysis revealed altered cardiac repolarization as evidenced by long QT and T-wave morphology changes [25]. The ECG abnormalities are observed both in vivo and ex vivo [33]. We noted, however, that the cardiac phenotype was pleiotropic since the mutation also increased P- and QRS-wave amplitudes, changes that have not been reported in JLNS patients. In addition to their deafness, the mice displayed an inner-ear-dependent behavioral phenotype called shaker/waltzer. To separate the ECG phenotype from the inner ear, we developed the RWS mouse model described in this report.

In humans, the missense mutations *A341E* and *T312I* of KCNQ1 are dominantly inherited, associated with syncope and cardiac arrest, and are linked to RWS. In vitro work demonstrates that when *A341E* and wild-type *KCNQ1* cRNA are injected together into *Xenopus* oocytes the mutation dominantly negatively affects channel function, leading to a 23% decrease in $I_{Ks}$ current [34]. When we introduce *A340E* into mouse *Kcnq1* the mutation dominantly negatively affects cardiac repolarization and produces a long QT phenotype concordant with the clinical and in vitro data (Fig. 5 and Table 1). Both heterozygous and homozygous *A340E* mice showed normal inner ear function as determined by auditory and vestibular tests (Figs. 3 and 4). Thus the *A340E* mice model RWS and clearly demonstrate that the long QT phenotype can be observed independent of inner ear dysfunction.

We should note that the sensitivity of the inner ear to the *A340E* function appears to be somewhat strain dependent. That is, as we have continued to interbreed subsequent generations, we have begun to notice litters that contain circling *Kcnq1*$^{A340E/A340E}$ animals. These mice may be useful for identifying genetic modifiers of potassium recycling in the inner ear. Importantly, their existence does not detract from our argument that inner ear dysfunction/hyperactivity and ECG abnormalities can be separated.

The *Kcnq1*$^{T311I/T311I}$ mice did not phenocopy RWS but rather resemble the *Kcnq1*$^{-/-}$ mice and hence model JLNS. First, heterozygous animals are asymptomatic. Second, homozygous mice are deaf, display shaker/waltzer behavior, and show a significant lengthening of the QT interval accompanied by changes in QRS amplitude and T-wave area (Table 1). By examination of *A340E* mice we have ruled out hyperactivity as a necessary contributor to long QT. However, in all our mice, the increased QRS amplitude is associated with hyperactivity. We suggest that this aspect of the ECG phenotype is secondary and associated with the decrease in body weight induced by hyperactivity (Table 2). The decreased body weight of *Kcnq1*$^{T311I/T311I}$ mice may be sufficient to explain the increased QRS amplitude on ECG, since the amount of subcutaneous fat tissue is known to influence QRS amplitude in humans[35].

Our studies do not address why the *T311I* and the *A340E* mutations induce distinct phenotypes in mice. Patients heterozygous for either allele present with RWS, while only mice heterozygous for A340E display a prolonged QT interval. There are no known patients homozygous for either mutation. Mice homozygous for *A340E* phenocopy RWS, while animals homozygous for *T311I* mimic JLNS. Altogether the results suggest that the *T311I* allele behaves essentially as a loss-of-function mutation while *A340E* acts as a dominant negative. Normal cardiac function may be more sensitive to disturbances in channel gating activity as the timing of channel function is critical. In the ear, Kcnq1 may be functioning more as a simple pore for $K^+$ extrusion. In any case, distinct and separate experiments examining structure–function of the Kcnq1 channel will be required to understand the molecular basis for the phenotypes associated with each point mutation.

In our previous report we demonstrated by startle response that *Kcnq1*$^{-/-}$ mice are deaf. Histological examination revealed a drastic reduction in the volume of endolymphatic space and a collapse of the membranous labyrinth in the vestibular and auditory apparatus. Lee et al. [26] noted these results while examining an independent knockout of *Kcnq1*. In addition they conducted ABR to measure auditory brain-stem activity. The wild-type and heterozygous mice had a normal hearing threshold, while *Kcnq1*$^{-/-}$ mice showed no response to the maximum level of auditory stimulation. A complete assessment of auditory function in *Kcnq1*$^{T311I/T311I}$ mice presented here corroborates previous analyses. Moreover, additional testing using DPOAE demonstrates the auditory defect is a result of hair cell failure, which is likely secondary to the collapse of the membranous labyrinth. Histological analyses indicate that this failure is almost certainly caused by the inability of the stria vascularis to produce and/or maintain endolymph, which is thus the primary defect in these mutant mice. The vestibular analysis quantifies the balance defect, which was previously described only in terms of behavior. Consistent with the functional data, histology of the inner ear shows that the deafness and balance defects result from the same abnormality: collapse of the membranous labyrinth, which may ultimately lead to degeneration of the hair cells.

It appears that complete loss of *Kcnq1* has a more profound affect on cardiac function than point mutagenesis. This is highlighted by the prevalent P-wave changes observed in *Kcnq1*$^{-/-}$ mice, which are absent in *A340E* and *T311I* point-mutant mice. The lack of P-wave changes in the hyperactive *Kcnq1*$^{T311I/T311I}$ mice implies that the atrial phenotype is not simply secondary to the inner ear dysfunction but suggests that Kcnq1 plays a role in atrial function. In humans there is growing clinical evidence that supports a role for Kcnq1 in atrial function. A recent report mapped a hereditary atrial fibrillation syndrome to the *KCNQ1* gene [36]. In addition, a study by Kirchhof et al. [37] uncovered altered atrial electrophysiology in patients with long QT syndrome. In the mouse, Kcnq1 is unlikely to function through association with Kcne1, since there appears to be little if any Kcne1 present in the atria and $I_{Ks}$ is undetectable in the atria during development [38,39]. However, Kcnq1 is capable of pairing with alternate β-subunits of the Kcne family (Kcne2 to Kcne5), thus producing a repertoire of currents with distinct electrophysiological properties [12–14,40]. Both *Kcne2* and *Kcne3* are expressed in the atria and could associate with Kcnq1 and contribute to its repolarization [39].

Mutations in mouse *Kcnq1* phenocopy human LQT1 in their abnormal ECGs. However, we have not detected mutation-associated atrial or ventricular arrhythmias in *Kcnq1*$^{-/-}$ knockout mice[33]. This is not altogether surprising since in humans it is apparent that mutations in *Kcnq1* only predispose patients to arrhythmias. Normally the heart beats with remarkable fidelity and arrhythmias are a rare occurrence; this has led to the multihit hypothesis, which suggests that additional hits (from drugs, stress, or genetic modifiers, for example) are necessary to induce cardiac arrhythmias in long QT patients [2]. The development of a mouse model with delayed ventricular repolarization in the absence of the confounding hyperactivity/circling phenotype will enable studies to look for such secondary hits in the mouse. Alternatively, such events may never be observed because of significant differences between mouse and human heart physiology.

One notable difference in cardiac physiology between the species is the lack of detectable $I_{Ks}$ in the adult mouse heart. Consistent with this finding, *Kcne1* mRNA levels become very low in the adult mouse; however, *Kcnq1* expression remains high [41,42]. Here, we demonstrate that a long QT phenotype is readily identified in several *Kcnq1* mutant mouse models, even in the absence of confounding behavioral abnormalities. Hence we believe that genetic and molecular analyses indicate that mouse Kcnq1 plays a significant role in cardiac function of the adult mouse apart from any contribution to $I_{Ks}$. Future studies will use the *Kcnq1*$^{-/-}$ mouse as a tool to uncover currents that rely on Kcnq1 in vivo in adult mice and the assessment of the roles, if any, these currents might have in human cardiac biology.

## Methods

### *Generating A340E, A340V, and T311I mice*

The three targeting vectors, pJV2, pJV3, and pJV4, are essentially identical except for the single base pair changes in exon 7 (Fig. 2). To construct these vectors we isolated a 9.5-kb *Eco*RI fragment from bacterial artificial chromosome BAC118L22 [42]. The 5′ *Eco*RI site lies 4.4 kb upstream of exon 7. The 3′ *Eco*RI site is not in the native *Kcnq1* gene but is actually derived from the polylinker sequences of the BAC vector. The 3′ flank includes exons 8, 9, and 10 of *Kcnq1* in a 5.0-kb fragment (ending at a *Hin*dIII site). To introduce the point mutations into the targeting vectors, we first subcloned the 2.6-kb *Sex*AI fragment carrying exon 7 and surrounding intronic sequences. A floxed *NeoR* gene was introduced at the unique *Bsm*I site inside intron 7, 60 bp from the 3′ end of exon 7. The point mutations *T311I* (ACC (Thr) → ATC (Ile)), *A340E* (GCA (Ala) → GAA (Glu)), and *A340V* (GCA (Ala) → GTA (Val)) were introduced using the Transformer Site-Directed Mutagenesis Kit (Clontech), essentially following the method of Deng and Nickoloff [43]. The entire *Sex*AI fragment was then sequenced before being returned to its original location in the 9.5-kb *Eco*RI clone. Targeting vectors also each carried the *diphtheria toxin A* (*DT-A*) gene for negative selection and were used to generate mutant mice as described for Fig. 2. Chimeric founders were crossed with C57BL/6 females

and Agouti animals were screened for the mutant chromosomes. Males carrying the targeted chromosome were mated with FVB/n females homozygous for a transgene insert with the Cre *recombinase* gene under control of the *EIIa* promoter [44]. Progeny in which the *NeoR* cassette was deleted were identified by PCR and these were mated with wild-type C57BL/6. Finally, males and females positive for the point mutations were intercrossed to generate animals for this study.

*RNA analysis*

*Kcnq1* RNA was prepared and quantified by Northern blot as previously described [42]. cDNAs were prepared using the SuperScript First-Strand Synthesis System for RT-PCR (Invitrogen). A 490-bp product was amplified using *Kcnq1*-specific primers (5′-CGATCGCCAGGGGGGTACC-3′ forward and 5′-CGTGTGACTCCGAGCAGGCT-3′ reverse).

*Auditory brain-stem responses and distortion product otoacoustic emission*

Mice were anesthetized with avertin and ABR measurements were recorded as described previously [45,46]. Cochlear function was tested via distortion product otoacoustic emissions as described by Lonsbury-Martin et al. [47]. Mice for this assay were generated as described above and tested at 8–10 weeks of age.

*Histological analysis*

Light microscope analyses of the cochlea and vestibular organs of the inner ear from 10-week-old mice were as described previously [45]. These mice represent a subset of those tested for ABR and DPOE responses.

*Gross evaluation of vestibular functions*

Mice were placed in a water bath at 37°C and allowed to swim and climb onto a dry platform. The swimming performance and the time taken to swim to the target were scored in a blind fashion. Balance was further tested using a custom-made setup as described [48]. Each animal's ability to balance on both the stationary and the rotating cylinder was scored. These are the same mice tested for ABR and DPOE responses.

*ECG analysis*

ECG measurements were obtained as previously described [25]. A single observer who was blinded to the genotype analyzed all ECG parameters. For each genotype approximately equal numbers of male and female mice were generated as described above and assayed at 13 to 22 weeks of age.

## Acknowledgments

This work was supported by grants to E.N.Y. (NIH-DC03828, DC04215) and B.C.K. (R01HL071670). This work was also supported by the intramural funds of the National Institute of Child Health and Human Development/NIH (K.P.).

## References

[1] R. Kass, A. Moss, Long QT syndrome: novel insights into the mechanisms of cardiac arrhythmias, J. Clin. Invest. 112 (2003) 8105.
[2] M. Keating, M. Sanguinetti, Molecular and cellular mechanisms of cardiac arrhythmias, Cell 104 (2001) 569–580.
[3] W. Wang, et al., SCN5A mutations associated with an inherited cardiac arrhythmia, long QT syndrome, Cell 80 (1995) 805–811.
[4] I. Splawski, M. Tristani-Firouzi, M. Lehmann, M. Sanguinetti, M. Keating, Mutations in the hminK gene cause long QT syndrome and suppress IKs function, Nat. Genet. 17 (1997) 338–340.
[5] M. Curran, et al., A molecular basis for cardiac arrhythmia: HERG mutations cause long QT syndrome, Cell 80 (1995) 795–803.
[6] G. Abbott, et al., MiRP1 forms IKr potassium channels with HERG and is associated with cardiac arrhythmia, Cell 97 (1999) 175–187.
[7] Q. Wang, et al., Positional cloning of a novel potassium channel gene: KVLQT1 mutations cause cardiac arrhythmias, Nat. Genet. 12 (1996) 17–23.
[8] P. Mohler, et al., Ankyrin-B mutation causes type 4 long-QT cardiac arrhythmia and sudden cardiac death, Nature 421 (2003) 634–639.
[9] W. Zareba, et al., Influence of genotype on the clinical course of the long-QT syndrome. International Long-QT Syndrome Registry Research Group, N. Engl. J. Med. 339 (1998) 960–965.
[10] Y. Melman, A. Krummerman, T. McDonald, KCNE regulation of KvLQT1 channels: structure–function correlates, Trends Cardiovasc. Med. 12 (2002) 182–187.
[11] T. Takumi, H. Ohkubo, S. Nakanishi, Cloning of a membrane protein that induces a slow voltage-gated potassium current, Science 242 (1988) 1042–1045.
[12] B.C. Schroeder, et al., A constitutively open potassium channel formed by KCNQ1 and KCNE3, Nature 403 (2000) 196–199.
[13] M. Grunnet, et al., KCNE4 is an inhibitory subunit to the KCNQ1 channel, J. Physiol. 542 (2002) 119–130.
[14] K. Angelo, et al., KCNE5 induces time- and voltage-dependent modulation of the KCNQ1 current, Biophys. J. 83 (2002) 1997–2006.
[15] J. Barhanin, et al., K(V)LQT1 and lsK (minK) proteins associate to form the I(Ks) cardiac potassium current, Nature 384 (1996) 78–80.
[16] M.C. Sanguinetti, et al., Coassembly of K(V)LQT1 and minK (IsK) proteins to form cardiac I(Ks) potassium channel, Nature 384 (1996) 80–83.
[17] D.C. Marcus, Z. Shen, Slowly activating voltage-dependent $K^+$ conductance is apical pathway for $K^+$ secretion in vestibular dark cells, Am. J. Physiol. 267 (1994) C857–C864.
[18] A. Jervell, F. Lange-Nielsen, Congenital deaf–mutism, functional heart disease with prolongation of the Q-T interval and sudden death, Am. Heart J. 54 (1957) 59–68.
[19] I. Splawski, K.W. Timothy, G.M. Vincent, D.L. Atkinson, M.T. Keating, Molecular basis of the long-QT syndrome associated with deafness, N. Engl. J. Med. 336 (1997) 1562–1567.
[20] I. Friedmann, G.R. Fraser, P. Froggatt, Pathology of the ear in the cardio-auditory syndrome of Jervell and Lange-Nielsen: report of a third case with an appendix on possible linkage with the Rh blood group locus, J. Laryngol. Otol. 82 (1968) 883–896.
[21] N. Neyroud, et al., A novel mutation in the potassium channel gene KVLQT1 causes the Jervell and Lange-Nielsen cardioauditory syndrome, Nat. Genet. 15 (1997) 186–189.

[22] M. Sakagami, et al., Cellular localization of rat Isk protein in the stria vascularis by immunohistochemical observation, Hear. Res. 56 (1991) 168–172.
[23] M. Nicolas, D. Dememes, A. Martin, S. Kupershmidt, J. Barhanin, KCNQ1/KCNE1 potassium channels in mammalian vestibular dark cells, Hear. Res. 153 (2001) 132–145.
[24] P. Wangemann, Z. Shen, J. Liu, K(+)-induced stimulation of $K^+$ secretion involves activation of the IsK channel in vestibular dark cells, Hear. Res. 100 (1996) 201–210.
[25] M.C. Casimiro, et al., Targeted disruption of the Kcnq1 gene produces a mouse model of Jervell and Lange-Nielsen syndrome, Proc. Natl. Acad. Sci. USA 98 (2001) 2526–2531.
[26] M.P. Lee, et al., Targeted disruption of the Kvlqt1 gene causes deafness and gastric hyperplasia in mice, J. Clin. Invest. 106 (2000) 1447–1455.
[27] D.E. Vetter, et al., Inner ear defects induced by null mutation of the isk gene, Neuron 17 (1996) 1251–1264.
[28] B.C. Knollman, et al., Isoproterenol exacerbates a long QT phenotype in *Kcnq1*-deficient mice: possible roles for human-like isoform 1 and IKS, J. Pharmacol. Exp. Ther. (2004) (in press).
[29] F.Y. Shalaby, et al., Dominant-negative KvLQT1 mutations underlie the LQT1 form of long QT syndrome, Circulation 96 (1997) 1733–1736.
[30] I. Splawski, et al., Spectrum of mutations in long-QT syndrome genes KVLQT1, HERG, SCN5A, KCNE1, and KCNE2, Circulation 102 (2000) 1178–1185.
[31] R. Jongbloed, et al., DHPLC analysis of potassium ion channel genes in congenital long QT syndrome, Hum. Mutat. 20 (2002) 382–391.
[32] S. Chen, et al., KCNQ1 mutations in patients with a family history of lethal cardiac arrhythmias and sudden death, Clin. Genet. 63 (2003) 273–282.
[33] T. Tosaka, et al., Nicotine induces a long QT phenotype in Kcnq1-deficient mouse hearts, J. Pharmacol. Exp. Ther. 306 (2003) 980–987.
[34] Z. Wang, et al., Functional effects of mutations in KvLQT1 that cause long QT syndrome, J. Cardiovasc. Electrophysiol. 10 (1999) 817–826.
[35] A. Masui, et al., Effect of subadipose tissue on the variables of signal-averaged electrocardiography in healthy subjects, Am. J. Cardiol. 71 (1993) 465–467.
[36] Y.H. Chen, et al., KCNQ1 gain-of-function mutation in familial atrial fibrillation, Science 299 (2003) 251–254.
[37] P. Kirchhof, et al., Prolonged atrial action potential durations and polymorphic atrial tachyarrhythmias in patients with long QT syndrome, J. Cardiovasc. Electrophysiol. 14 (2003) 1027–1033.
[38] M.P. Davies, et al., Developmental changes in ionic channel activity in the embryonic murine heart, Circ. Res. 78 (1996) 15–25.
[39] D. Franco, et al., Divergent expression of delayed rectifier K(+) channel subunits during mouse heart development, Cardiovasc. Res. 52 (2001) 65–75.
[40] N. Tinel, S. Diochot, M. Borsotto, M. Lazdunski, J. Barhanin, KCNE2 confers background current characteristics to the cardiac KCNQ1 potassium channel, EMBO J. 19 (2000) 6326–6330.
[41] M.D. Drici, et al., Involvement of IsK-associated $K^+$ channel in heart rate control of repolarization in a murine engineered model of Jervell and Lange-Nielsen syndrome, Circ. Res. 83 (1998) 95–102.
[42] T.D. Gould, K. Pfeifer, Imprinting of mouse Kvlqt1 is developmentally regulated, Hum. Mol. Genet. 7 (1998) 483–487.
[43] W.P. Deng, J.A. Nickoloff, Site-directed mutagenesis of virtually any plasmid by eliminating a unique site, Anal. Biochem. 200 (1992) 81–88.
[44] M. Lakso, et al., Efficient in vivo manipulation of mouse genomic sequences at the zygote stage, Proc. Natl. Acad. Sci. USA 93 (1996) 5860–5865.
[45] P.J. Kozel, et al., Balance and hearing deficits in mice with a null mutation in the gene encoding plasma membrane $Ca^{2+}$-ATPase isoform 2, J. Biol. Chem. 273 (1998) 18693–18696.
[46] M. Flagella, et al., Mice lacking the basolateral Na–K–2Cl cotransporter have impaired epithelial chloride secretion and are profoundly deaf, J. Biol. Chem. 274 (1999) 26946–26955.
[47] B.L. Lonsbury-Martin, M.L. Whitehead, Distortion product otoacoustic emissions, in: M.S. Robinette, T.J. Glattke (Eds.), Otoacoustic Emissions: Clinical Applications, Thieme, New York, 1997, pp. 83–109.
[48] M. Xiang, et al., Essential role of POU-domain factor Brn-3c in auditory and vestibular hair cell development, Proc. Natl. Acad. Sci. USA 94 (1997) 9445–9450.